

**DESCRIPTION AND ANALYSIS OF INFRASOUND AND SEISMIC SIGNALS RECORDED FROM THE
WATUSI EXPLOSIVE EXPERIMENT, SEPTEMBER 2002**

Joydeep Bhattacharyya,¹ Henry E. Bass,² Douglas P. Drob,³ Rodney W. Whitaker,⁴
Douglas O. Revelle,⁴ and Thomas D. Sandoval⁴

Science Applications International Corporation;¹ National Center for Physical Acoustics;²
Naval Research Laboratory;³ Los Alamos National Laboratory⁴

Sponsored by Army Space and Missile Defense Command and
National Nuclear Security Administration
Office of Nonproliferation Research and Engineering
Office of Defense Nuclear Nonproliferation

Contract No. DASG60-03-0009^{1,2,3} and W-7405-ENG-36⁴

ABSTRACT

The Watusi test was conducted at 21:25 UTC on 28 September 2002 at the Nevada Test Site (NTS). At that time, 19 tons of TNT equivalent were detonated in a cylindrical container that was partially above ground level. The resulting infrasound signal was recorded clearly at seven infrasound stations from nearby station NTS to the International Monitoring System (IMS) station I10CA located 2165 km from the test. No observations were made at two stations closer to the event than I10CA, i.e., TXIAR and I57US, suggesting significant variations in atmospheric conditions and/or station noise levels. The seismic observations were limited to distances less than 250 km though we do not note any significant azimuthal variation of detection in this dataset. Such a distance limitation makes infrasound technology better suited to detect small surface explosions. For each infrasound array, we estimate the arrival time and duration, dominant period and the peak-to-peak amplitude of the detected signals. For the array analysis, the window length and the overlap between consecutive windows and the frequency range of the analysis were adjusted depending on the nature of the signal, the signal-to-noise ratio (*SNR*) and to a certain extent, the distance from the source. The signal duration scales approximately with distance, though we observe no clear relationship between distance and the dominant period of the signal. We undertake forward modeling exercises to verify the ability of atmospheric propagation models to predict the travel times and amplitudes of the infrasound signals. Following ray tracing using realistic atmospheric models, we note that the travel times are slightly better predicted by a real-time environmental model like *G2SRT* compared to a climatological model like *HWM/MSISE-00*, though due to limitations in our modeling tool, we could only use range independent profiles in the former case. Based on the predicted travel times of various infrasound phases, we note that most of our observations are of thermospheric paths. Using time independent parabolic equation calculations we could qualitatively verify the lateral variation of observed amplitudes. The variation of wind corrected amplitude with distance range is consistent with those from large-scale explosions carried out at the White Sands Missile Range. We hope the Watusi data, which has been distributed publicly to the infrasound community will provide a framework for testing theoretical predictions using realistic conditions.

OBJECTIVES

This paper presents the Watusi explosion data and analysis that augments Whitaker *et al.* (2002) with additional infrasound and seismic observations, forward modeling that tests our ability to predict the infrasound signals, and a preliminary analysis of the amplitudes of these observations.

RESEARCH ACCOMPLISHED

The Watusi explosion was detonated at 21:25:17 UTC on of September 28, 2002 at the Nevada Test Site (NTS) (37.099° N, 116.092° W). A cylindrical container that was partially above ground level held the 38,000 pounds (0.019 kT) of TNT equivalent. The acoustic wave was recorded clearly at seven infrasound stations at distances ranging from 45 km (station NTS) to 2,165 km (IMS station I10CA). Signals were not detected at stations I57US at a distance of 390 km and TXIAR at a distance of 1,440 km; both south of the source (Table 1, Figure 1).

Table 1. Infrasound stations used in the analysis.

Station	Location (°)	Distance (km)	Signal Detected	Observed Azimuth(°)
NTS	36.7056 N, 115.9631 W	45	Yes	352.77
SGAR	37.0153 N, 113.6153 W	219	Yes	277.27
NVIAR	38.4296 N, 118.3030 W	244	Yes	128.99
I57US	33.6058 N, 116.4532 W	390	No	
PDIAR	42.7663 N, 109.5939 W	838	Yes	218.06
LSAR	35.8670 N, 106.3340 W	883	Yes	294.08
DLIAR	35.8670 N, 106.3340 W	883	Yes	285.64
TXIAR	29.3338 N, 103.6670 W	1,440	No	
I10CA	50.2010 N, 96.0270 W	2,165	Yes	230.44

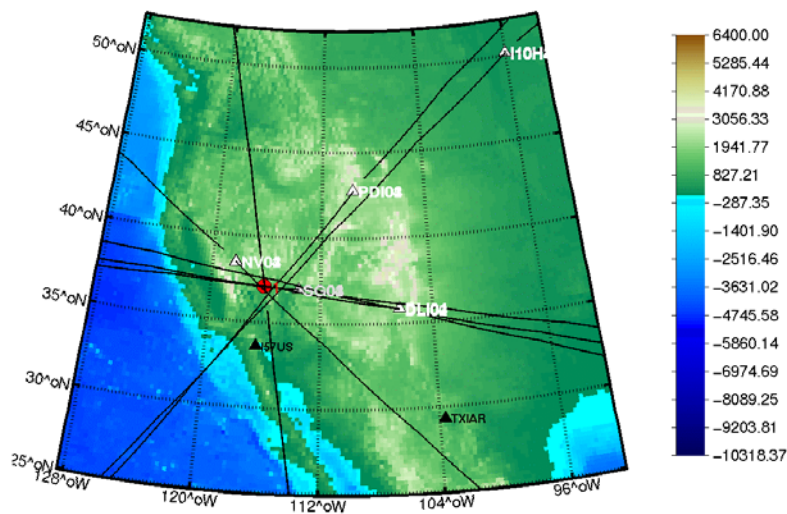


Figure 1. Infrasound stations, the Watusi explosion, and observed azimuths. Elevations are in meters. I57US and TXIAR did not detect Watusi.

Observed Waveforms

Array processing results and samples of the observed waveforms for the nearest (NTS) and furthest (I10CA) stations that clearly recorded signals from the Watusi event are shown in Figure 2. The top panel shows the F-statistic (*Fstat*), which is a measure of the presence of the coherent signal. The second and third panels show the observed signal velocity across the array and the observed back-azimuth to the source. Consistent velocities and back-azimuth estimates, coupled with distinctly higher *Fstat* values identify the start and duration of the detections that are shown as shaded regions in the top three panels. The bottom panel shows examples of filtered waveforms.

The array analysis parameters (window lengths, overlaps, and frequency ranges) were adjusted for optimal results. Typically, the data were filtered between 0.5–3.0 Hz using a 20-s window and a 50% overlap. For the nearby NVIAR and NTS stations, the data were filtered between 1–3 Hz, and for the distant I10CA station, the frequency band was 0.5–2 Hz and a 100-s window was used.

Stations LSAR and DLIAR are nearly co-located (within a few hundred meters of each other) at a distance of 883 km from the source. The energy incident on the two arrays from the explosion was assumed to be the same, but the waveforms at LSAR had higher amplitudes than those at DLIAR did. The LSAR array is smaller than the DLIAR array; so lower correlation values are expected (and observed) for frequencies above 1.5 Hz at DLIAR. The duration of the explosion signal for these two stations was similar.

The explosion signal lasts only a few seconds at NTS (Figure 2) but the duration of the explosion signal at I10CA is several minutes. Longer duration signals are expected at larger distances because acoustic energy is returned to the receiver from different layers of the atmosphere. Although the trace velocities and *Fstat* values were not always stable, the azimuths were reasonably constant and crossed near the source location for each station (Figure 1).

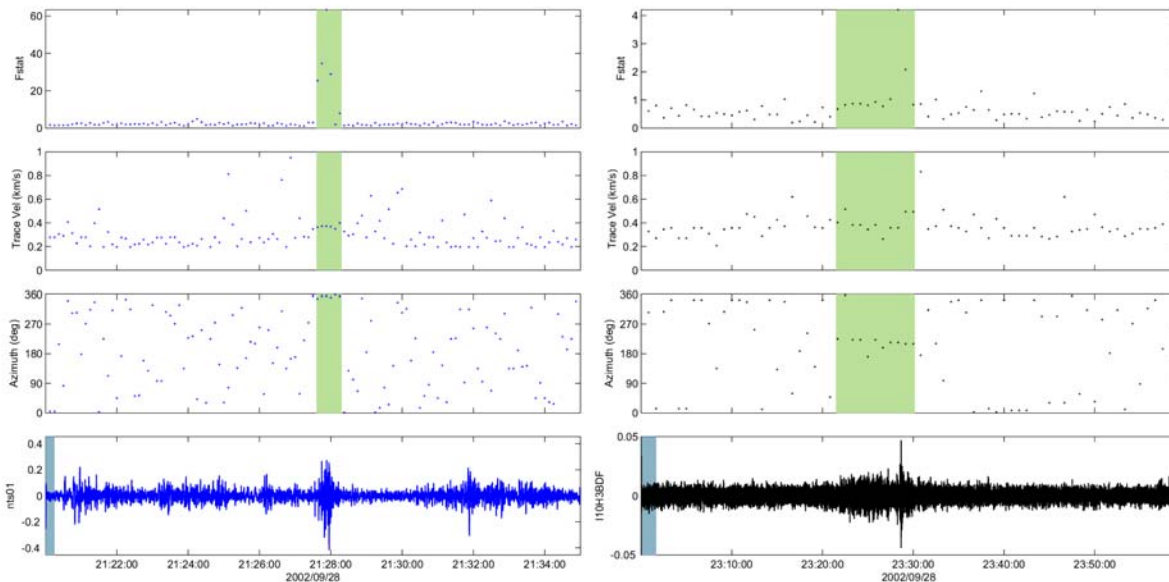


Figure 2. Acoustic signals from the Watusi explosion as recorded at NTS (45 km from the source, left panels) and I10CA (2,165 km from the source, right panels). The NTS data were filtered between 0.5–3.0 Hz and the signal amplitude is in volts. The I10CA data were filtered between 0.5–2.0 Hz and the signal amplitude is in Pascals. The shaded box indicates the detected infrasound signal.

Table 2 gives the maximum single-cycle peak-to-peak signal amplitude measured at each station. The amplitudes from all the sensors at a single station were averaged to determine the amplitudes reported. At PDIAR the signal amplitude from two of the sensors were up to 40% larger than the remaining two sensors. It is not clear if this was caused by different local meteorological conditions or poor calibration. The amplitude estimates from PDIAR are less reliable than the other estimates.

Table 2. Measured and wind-corrected amplitudes for acoustic waveforms.

Station	Measured Amplitude (μbar)	Wind (m/s)	Wind Corrected Amplitude (μbar)	Distance from Source (km)
NTS	3.20			45
SGAR	4.10	11.6	1.60	219
NVIAR	0.35	-6.6	0.62	244
PDIAR	0.44	31.0	0.78	838
LSAR	0.60	11.1	0.24	883
DLIAR	0.70	11.1	0.24	883
I10CA	0.82	27.8	0.13	2,165
TXIAR	-	-4.7	0.06	1,440
I57US	-	-10.0	0.28	390

Table 2 also shows an estimate of the wind-corrected amplitude. Whitaker (1995) developed an empirical expression that relates acoustic pressure, P , in Pascals to the yield, W , in kT, distance, R , in km, and wind velocity, v , in m/sec,

$$\log(P) = 3.37 + 0.68 \log(W) - 1.36 \log(R) + 0.019 v \quad (1)$$

The vector wind velocity shown in Table 2 was computed from wind profiles and is the wind in the direction of propagation at 50-km elevation. Figure 3 shows wind-corrected amplitudes as a function of scaled range. The pressure values are given as the maximum peak-to-peak amplitude divided by $10^{(0.019v)}$. The scaled range is given by $(\text{distance}/\sqrt{(2 \times \text{yield})})$, where the yield for the Watusi explosion is 0.019 kT.

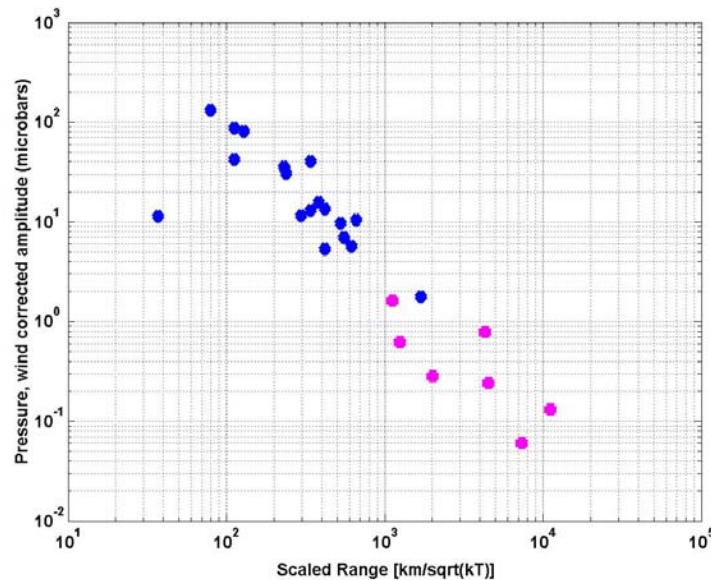


Figure 3. Wind-corrected amplitudes for Watusi (light symbols) and other explosive tests (dark symbols).

The dark symbols in Figure 3 were obtained from Davidson and Whitaker (1992) and from a series of large-scale explosive tests at White Sands Missile Range. The range of infrasonic measurements for those events was from 250 km to 5,300 km. The values for the Watusi experiment are shown by the light symbols.

The Watusi explosion measurements follow the trend of the data from the other explosions plotted in Figure 3. However, the maximum peak-to-peak amplitudes used for this comparison may not be an adequate measure. As the signal propagates it is dispersed by multiple paths and frequency dependent velocity and absorption. The acoustic energy received at any location might be represented well by an integral over the entire waveform.

Meteorological Modeling

Acoustic signal travel times and amplitudes are functions of the meteorological conditions. Near the source, most of the acoustic energy is along a direct path near the ground. At greater distances, however, signals propagate into the stratosphere or thermosphere (or both) and return to the surface if the meteorological conditions are favorable. Accurate travel time prediction requires knowledge of the atmospheric conditions along the propagation path.

Table 3 lists the observed travel time and signal duration as well as travel times computed using different atmospheric models. The predicted travel times were calculated using a ray trace routine (Gibson and Norris, 2002). Two different atmospheric profiles were tested: the Mass Spectrometer and Incoherent Scatter Radar empirical model (NRLMSISE-00) combined with the Horizontal Wind Model (HWM-93), and the Naval Research Laboratory Ground to Space (NRL-G2S) semi-empirical spectral model (Drob *et al.*, 2003). For the NRL-G2S calculation, the range-averaged effective sound speed was used. The G column contains the travel times predicted for a wave propagating near the surface (the ground wave). The travel times of these waves are the great circle distance divided by the nominal speed of sound near the surface. The columns labeled S and T are the travel times predicted for returns from the stratosphere and thermosphere, respectively. Two entries for thermospheric arrivals imply that two ray paths are predicted.

Table 3. Observed and predicted acoustic travel times for the Watusi event.

Station	Observed (time, duration)		Predicted (HWM-93/NRLMSISE-00)			Predicted (NRL-G2S)		
			G	S	T	G	S	T
NTS	160 s	25 s	136	-	-	113	-	-
SGAR	776 s	35 s	663	-	793	643	-	777
NVIAR	841 s	30 s	740	-	1,153	717		1,146
PDIAR	2,691 s	220 s	2,539	-	3,052	2,445	-	2,805
DLIAR	2,886 s	115 s	2,676	-	3,215 3,668	2,597	*	3,223
LSAR	2,893 s	110 s	2,676	-	3,215 3,668	2,597	*	3,223
I10CA	7,390 s	500 s	6,560	-	7,459 8,197	6,395	-	7,047

* Stratospheric arrivals are seen with less stringent eigen-ray conditions.

Wind and temperature as a function of altitude were predicted along the great circle path (GCP) from source to receiver using both HWM-93/NRLMSISE-00 and NRL-G2S models. Temperature and wind profiles computed from the NRL-G2S model are shown in Figure 4 for the path from Watusi to PDIAR. Atmospheric profiles were computed at ten equally spaced points from the source to the receiver. These profiles were then averaged to produce range-independent profiles for the forward calculations. Average values were used for the NRL-G2S model because the modeling software was limited to range-independent profiles for models other than HWM-93/NRLMSISE-00. The HWM-93/NRLMSISE-00 ray simulations were range-dependent by default.

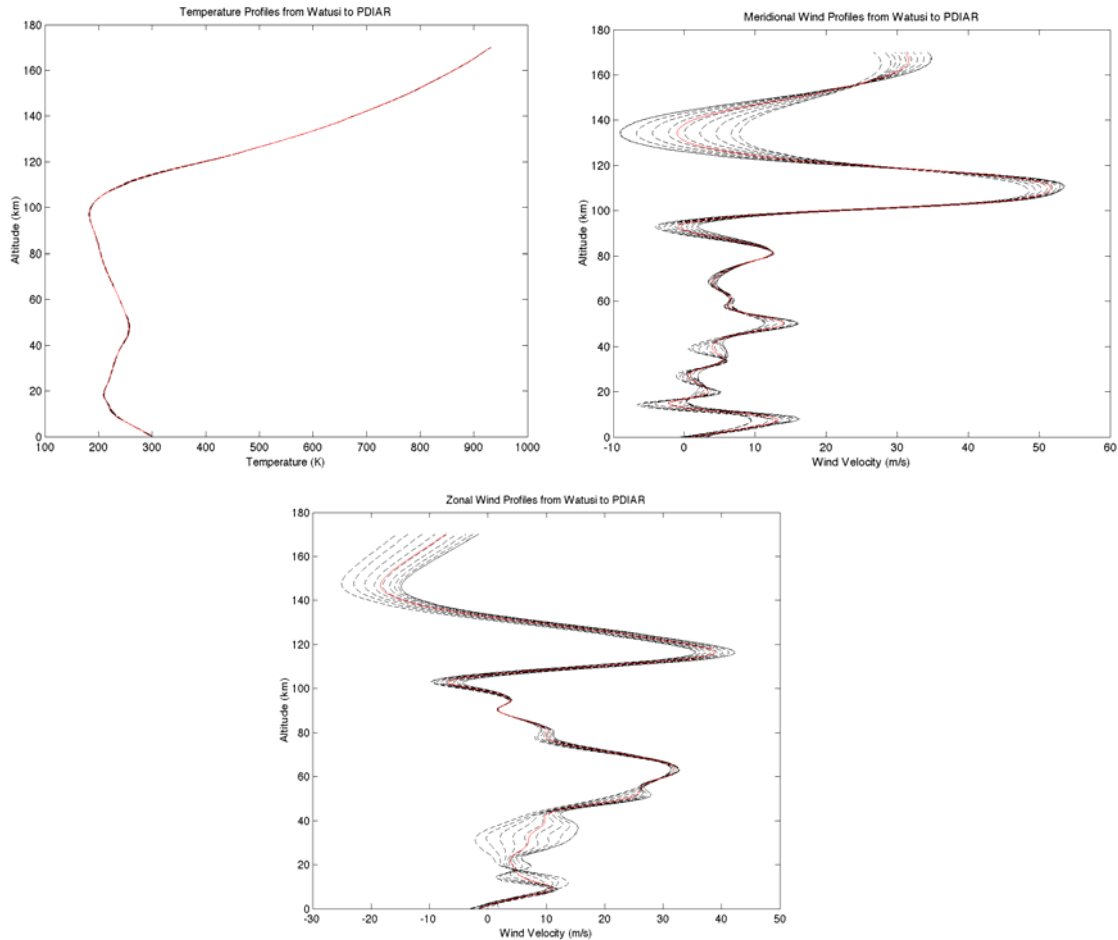


Figure 4. Temperature (upper left), meridional wind speed (upper right), and zonal wind speed (bottom) for ten vertical profiles along the great circle path from source to receiver from model NRL-G2S.

A range-independent approach is questionable because ray-path deviations close to the source can have a significant effect on the travel time. Thus, the calculations based upon range-independent profiles using NRL-G2S are considered preliminary.

The temperature profile from the source to PDIAR does not change dramatically along the great circle path but the winds do (Figure 4). This is common. The wind profiles are largely responsible for the variation in propagation conditions on time scales of several hours to several days. These effects are observed in daily measurements of Concorde bow shock arrivals (Le Pichon *et al.*, 2002). Several detailed theoretical studies have investigated the importance of wind variability on infrasound propagation (Garces *et al.*, 1999, 2002; Drob *et al.*, 2003).

For the HWM-93 model the predicted meridional wind component below 60 km is zero. This is because climatologically, the average meridional wind velocity is near zero. A monthly average is a poor approximation compared to daily data. For example, the HWM model would not predict a tropospheric or stratospheric duct in a predominantly meridional direction. Above 75 km the NRL-G2S and HWM/MSISE specifications are virtually identical.

Signal Amplitudes

The measured amplitudes are reasonably well predicted by the LANL empirical relation (Whitaker, 1995). The amplitude at the receiver can also be predicted from calculations that include full wave effects. The signal loss from a reference point to the measurement point is predicted by Parabolic Equation solutions (Figure 5).

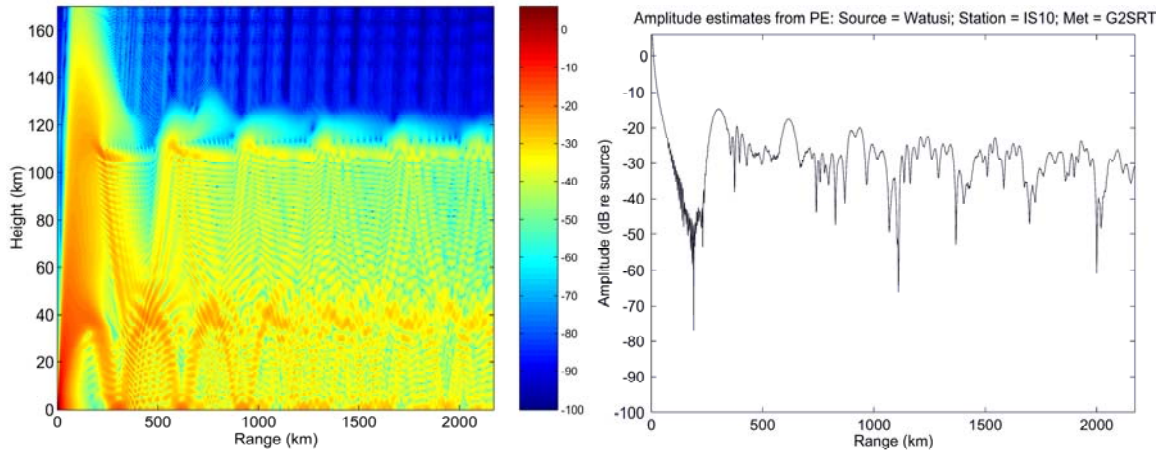


Figure 5. The acoustic field predicted by the PE calculation as a function of height and at the surface. The amplitude units are in dB relative to the amplitude at 10 km from the source. Model NRL-G2S was used for the calculations.

The predicted surface amplitudes qualitatively agree with the observation. Beyond 700 km the amplitude decreases with range very slowly, but inside of 200 km the amplitude decreases dramatically with distance. The interference dip near 200 predicts reduced amplitudes due to turbulence, but the measured signal amplitude at SGAR (219 km) is a little larger than that measured at NTS (45 km). At a range of about 800 km, there are fluctuations with range that are larger than the mean difference between signal amplitudes predicted at ranges of 800 km and 2,200 km. These fluctuations explain the relative amplitudes observed at PDIAR, DLIAR, and I10CA. The measured signal amplitude is smaller at PDIAR than at DLIAR, even though PDIAR is nearer to the event, and the signal amplitude at I10CA is greater than either PDIAR or DLIAR.

Single Station Estimates of Range Using Seismic and Infrasonic Data

The IMS infrasound network is sparse. For events with source sizes comparable to Watusi, only one IMS infrasound station will possibly detect the signal. Combining seismic and infrasound data from the same event can improve location estimates when a single infrasound station detects the event.

The Watusi explosion was a relatively small event. The only co-located seismic and infrasound array stations that both recorded signals associated with the explosion were in Mina, Nevada (seismic station NVAR and infrasound station NVIAR). The back-azimuth estimates from the two datasets were consistent. Using t_a as the travel time for the infrasound energy, t_p as the travel time for the seismic P wave, V_a as the velocity of the acoustic wave (300 m/s), and V_p as the average speed of the P wave, the distance from source to receiver is given by equation (2):

$$D = V_a t_a = V_p t_p \quad (2)$$

The value of V_p used was 6.18 km/s. Although D and t_p were used to estimate V_p in this case, the average seismic velocity near Mina could have been obtained from independent data recordings of nearby earthquakes. The distance to the event is insensitive to the average P-wave velocity (an error of 0.5 km/s would change the distance by about 1 km) so the use of an exact P-wave velocity does not alter the conclusions. The travel-time difference between the P-wave and the acoustic wave, $t_a - t_p$, measured at NVAR was 784 s. Solving for D gives 247.4 km; close to the correct value of 244.5 km. This example illustrates how combined seismic and acoustic sensor technologies can be used to locate (with back-azimuth estimates obtained from infrasound data) relatively small events recorded by a sparse network.

Analysis of Seismic Data

Seismic data from six western US seismic stations were analyzed for the Watusi explosion. Table 4 lists observations from the seismic stations that recorded arrivals from Watusi. Figure 6 shows the geographical distribution of these stations. Seismic arrivals were observed for stations up to about 250 km from the source. Unlike the infrasound observations, there is no clear azimuthal dependence of the seismic observations. Figure 6 shows the seismic arrival at the closest station, TPNV.

Table 4. Observations from the seismic stations recording Watusi.

Station	Lat., Long. (deg)	Arrival Time (GMT)	Dist (km)	BAZ (deg)	V (km/s)	Site
TPNV	36.9488 -116.2495	21:25:22.671	21.8	39.9	3.49	Topopah Spring Nevada
SHP	36.5055 -115.1602	21:25:36.639	106.6	308.7	5.42	Sheep Range, Nevada
TPH	38.0750 -117.2225	21:25:44.138	147.3	136.9	5.42	Tonopah, Nevada
MPM	36.0580 -117.4890	21:25:47.312	169.7	46.8	5.61	Manuel Prospect Mine, California
NEN (Pn)	35.6495 -114.8433	21:25:53.049	196.4	325.3	5.44	Nelson, Southern Nevada
NEN (Sn)	35.6495 -114.8433	21:26:16.739	196.4	325.3	3.28	Nelson, Southern Nevada
NVAR (Pn)	38.4296 -118.3036	21:25:56.572	244.5	126.5	6.18	Mina Array, Nevada
NVAR (Sn)	38.4296 -118.3036	21:26:30.497	244.5	126.5	3.32	Mina Array, Nevada

Of the six seismic stations, NVAR is the only array and the arrivals can be clearly associated to the Watusi event. For the other 3-component stations, the arrival-times and back-azimuths are consistent with Watusi. The group velocity increases with distance because the seismic wave detected at the farther stations has sampled deeper regions of the Earth. The Sn waveform is clearly observable only at the farthest two stations. From this limited sampling, the (V_p/V_s) ratio varies significantly for paths to the north and south of Watusi. Conversely, the Pn travel time can be anomalously early at NVAR

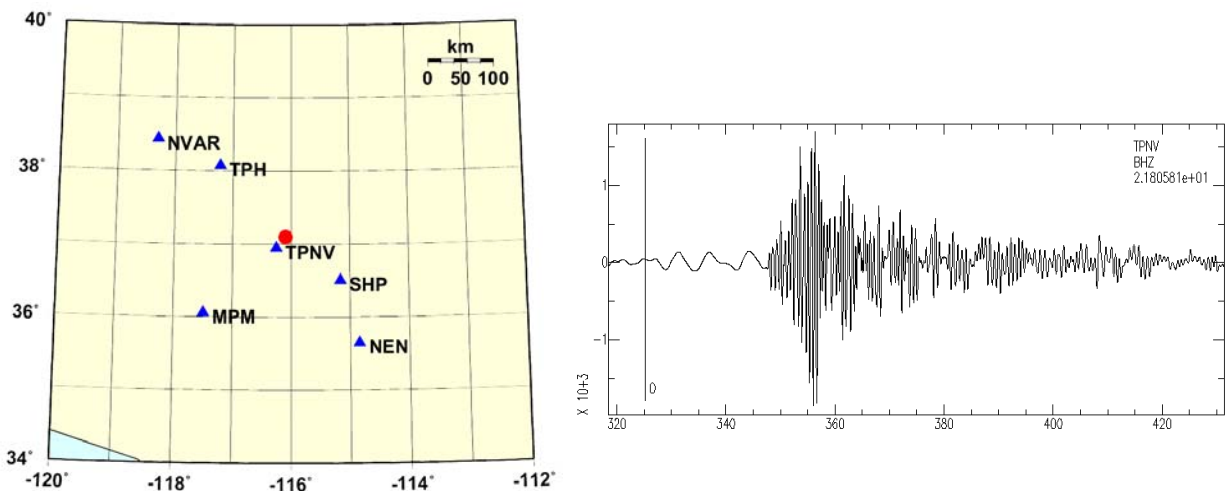


Figure 6. Locations of seismic stations that detected the Watusi event (circle) and an example waveform from station TPNV (21.8 km from the event).

CONCLUSIONS AND RECOMMENDATIONS

The waveform data, well-estimated meteorological profiles, and the ground-truth information make Watusi one of the best-characterized infrasound events available. The tools available to model the signal are not sufficient. For example, the amplitude cannot be predicted other than with an empirical relation. Travel times are only qualitative because the basis for the predicted values, raytracing, makes assumptions that are not fulfilled in this case. Hopefully, the Watusi data will provide an experimental dataset that can be used to test theoretical predictions of more realistic simulations.

Estimating source size

Prior investigators found that the period of the recorded acoustic wave in the far field scales with the size of the charge. Specifically, ReVelle (1980) finds that the observed period at maximum signal amplitude in seconds (T) for stratospheric returns is related to the known source energy (E in kT of TNT) by:

$$\log (E/2) = 3.34 \log (T) - 2.58 \quad (3)$$

For the Watusi data, zero crossings were counted to determine periods of 1 s for SGAR, 1.1 s for PDIAR, 1.2–2 s for NVIAR, and 1.1–1.9 s for I10CA for the un-filtered data. The average period was about 1.35 s, which gives an estimated yield of 0.014 kT. The range of yields varied between 0.0097 and 0.053 kT. The average was close to the true yield but the large variation suggests that result might simply be fortuitous.

Using normal mode calculations to predict infrasonic arrivals

A preliminary analysis of signal propagation using normal mode codes was performed with encouraging results. These codes predict both arrival times and signal amplitudes. A significant improvement in the predicted travel times was obtained using the Pierce normal mode code. However, the observed amplitudes were poorly predicted by the calculations. Research on this topic will benefit from the data produced by the Watusi experiment.

Null observation of Watusi at I57US

The location of the Watusi event was less than 400 km from I57US (Figure 1), which was less than the distance to several of the stations that detected the event. One possible reason for the null observation at I57US is that the wind patterns were not favorable for stratospheric or thermospheric propagation. The noise levels at the station might also have contributed to the null observation. Figure 7 shows the noise spectrum at I57US for the time window between 21:15 and 21:45 on the day of the event. This time window brackets the expected arrival time of the acoustic signal. Between 0.5–3.0 Hz the noise level is about 0.1 Pascal or 1 mbar. The predicted amplitude at I57US is much smaller than 1 mbar (see Table 2), so the absence of the signal for the Watusi explosion at I57US is expected.

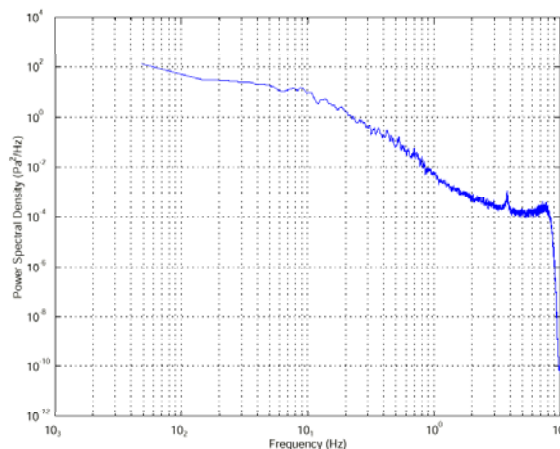


Figure 7. Noise levels at station I57US during the time of Watusi.

Ability of automatic infrasound processing algorithms to detect Watusi

Automated processing routinely analyzes waveforms recorded at SGAR, PDIAR, DLIAR and I10CA stations but only detected the signals at SGAR (even though the signals related to Watusi were clear at all of these stations). This suggests that improvements are needed in the automated detection parameters or their methods. Despite this detection failure, it is encouraging that an explosion with an equivalent yield of only 0.019 kT provided a clearly observable signal at a distance of 2,165 km. With reliable detections at this distance relatively small surface explosions like Watusi can be monitored with a sparse infrasound network.

ACKNOWLEDGEMENTS

Michael Hedlin performed the I57US noise analysis. We thank Bob North and Bob Woodward for comments on this report, Victoria Oancea and Paul Piraino for their help in obtaining both the infrasound and seismic datasets respectively, and Alysa Gorham for formatting the manuscript. Discussions with David Norris and Rob Gibson improved on this analysis.

REFERENCES

- Davidson, M. and R. W. Whitaker (1992), "Miser's Gold", LA-12074-MS (available at <http://lib-www.lanl.gov/cgi-bin/getfile?00818199.pdf>).
- Drob, D. P., J.M. Picone, and M.A. Garces (2003), The spatiotemporal variability of infrasound path partitioning, *J. Geophys. Res.*, accepted for publication.
- Garces, M., D.P. Drob, and J.M. Picone (2002), A theoretical study of the effects of geomagnetic fluctuations and solar tides on the propagation of infrasonic waves in the upper atmosphere, *Geophys. J. Int.*, **148**, 77–87.
- Garcés, M., R. Hansen, K. Lindquist, D. Drob, and M. Picone (1999), Variability of the lower atmosphere and its effect on the propagation of infrasonic waves, Proceedings of the 21st, Annual Research Symposium on Monitoring a Comprehensive Test Ban Treaty, US Government Printing Office.
- Gibson, R. and D. Norris (Oct 2002), Development of an Infrasound Propagation Modeling Tool Kit, Defense Threat Reduction Agency Technical Report, DTRA-TR-99-47, Ft. Belvoir, VA.
- Le Pichon, A., M. Garcés, E. Blanc, M. Barthélémy, and D. Drob, (2002), Acoustic propagation and atmosphere characteristics derived from infrasonic waves generated by the Concorde, *J. Acoust. Soc. Am.*, **111** (1), 629–641.
- Picone, J.M., A.E. Hedin, D.P. Drob, and A.C. Aikin (2002), NRLMSISE-00 Empirical model of the atmosphere: statistical comparisons and scientific issues, *J. Geophys. Res.*, **107** (A12): art. no. 1468.
- Revelle, D.O. (1980), Interaction of Large Bodies with the Earth's Atmosphere, in *IAU Symposium #90 Solid Particles in the Solar System*, edited by I. Halliday and B.A. McIntosh, D. Reidel Pub Co., Dordrecht, 185–198.
- Whitaker, R. (1995), Infrasonic Monitoring, Proceedings of the 17th Annual Seismic Research Symposium in Scottsdale, AZ, September 12–15, 997-1000.
- Whitaker, R.W., T.D. Sandoval, and D.O. Revelle (2002), Infrasonic observations of the Watusi explosive test, Infrasound Technology Workshop, De Bilt, The Netherlands.